Available online at www.sciencedirect.com
ScienceDirect
Journal of Magnetic Resonance 190 (2008) 222–232
JMR Journal of Magnetic Resonance
www.elsevier.com/locate/jmr

Electron spin relaxation enhancement measurements of interspin distances in human, porcine, and *Rhodobacter* electron transfer flavoprotein–ubiquinone oxidoreductase (ETF–QO)

Alistair J. Fielding [a], Robert J. Usselman [a], Nicholas Watmough [b], Martin Simkovic [c,1], Frank E. Frerman [c], Gareth R. Eaton [a], Sandra S. Eaton [a,*]

[a] *Department of Chemistry and Biochemistry, University of Denver, Denver, CO 80208-2436, USA*
[b] *Center for Metalloprotein Spectroscopy and Biology and School of Biological Sciences, University of East Anglia, Norwich NR4 7TJ, UK*
[c] *Department of Pediatrics, University of Colorado School of Medicine, Denver, CO 80262, USA*

Received 3 April 2007; revised 20 October 2007
Available online 6 November 2007

Abstract

Electron transfer flavoprotein–ubiquinone oxidoreductase (ETF–QO) is a membrane-bound electron transfer protein that links primary flavoprotein dehydrogenases with the main respiratory chain. Human, porcine, and *Rhodobacter sphaeroides* ETF–QO each contain a single $[4Fe–4S]^{2+,1+}$ cluster and one equivalent of FAD, which are diamagnetic in the isolated enzyme and become paramagnetic on reduction with the enzymatic electron donor or with dithionite. The anionic flavin semiquinone can be reduced further to diamagnetic hydroquinone. The redox potentials for the three redox couples are so similar that it is not possible to poise the proteins in a state where both the $[4Fe–4S]^{+}$ cluster and the flavoquinone are fully in the paramagnetic form. Inversion recovery was used to measure the electron spin-lattice relaxation rates for the $[4Fe–4S]^{+}$ between 8 and 18 K and for semiquinone between 25 and 65 K. At higher temperatures the spin-lattice relaxation rates for the $[4Fe–4S]^{+}$ were calculated from the temperature-dependent contributions to the continuous wave linewidths. Although mixtures of the redox states are present, it was possible to analyze the enhancement of the electron spin relaxation of the FAD semiquinone signal due to dipolar interaction with the more rapidly relaxing $[4Fe–4S]^{+}$ and obtain point-dipole interspin distances of 18.6 ± 1 Å for the three proteins. The point-dipole distances are within experimental uncertainty of the value calculated based on the crystal structure of porcine ETF–QO when spin delocalization is taken into account. The results demonstrate that electron spin relaxation enhancement can be used to measure distances in redox poised proteins even when several redox states are present.

Keywords: Electron spin relaxation enhancement; Interspin distance; Iron–sulfur cluster; ETF–QO; Flavoquinone

1. Introduction

Electron transfer flavoprotein–ubiquinone oxidoreductase (ETF–QO) [1–3] serves as the membrane-bound electron transport link to the main mitochondrial respiratory chain for electrons derived from the flavoprotein dehydrogenases that function in the oxidation of fatty acids and some amino acids in mammalian mitochondria. ETF–QO has two redox-active centers, a $[4Fe–4S]^{+,2+}$ cluster and FAD, and a binding site for ubiquinone, the electron acceptor. Ubiquinone was not present in the proteins isolated for this study. Porcine and human ETF–QO have 98% sequence identity, whereas human and *Rhodobacter sphaeroides* ETF–QO ETF–QO have 67% sequence identity [4,5]. An algorithm predicts $\leqslant$0.7 root mean square deviation/Å in the cores of the three proteins based on the high degree of sequence identity [6]. Consistent with the similarity in sequences, EPR *g*-values are comparable for the

* Corresponding author. Fax: +1 303 871 2254.
E-mail address: seaton@du.edu (S.S. Eaton).
[1] Present address: Department of Biochemistry and Microbiology, Faculty of Chemical and Food Technology, Slovak University of Technology, Radlinskeho 9, 81237 Bratislava, Slovak Republic.

1090-7807/$ - see front matter © 2007 Elsevier Inc. All rights reserved.
doi:10.1016/j.jmr.2007.11.002

$[4Fe–4S]^{+}$ in mammalian ETF–QOs [1,3,7] as are the redox potentials of porcine and *Rhodobacter* ETF–QO [5]. Thus, it is probable that the *Rhodobacter*, human, and porcine ETF–QOs have similar structures.

Titration of ETF–QO with octanoyl-CoA reduces the protein by two electrons in the presence of catalytic concentrations of medium-chain acyl-CoA dehydrogenase and ETF. The redox potentials relative to the standard hydrogen electrode at pH 7.5 and 4 °C are $E_1^{o'} = +0.028$ V and $E_2^{o'} = -0.006$ V for the first and second electron transfers, respectively, to the FAD and $E^{o'} = +0.047$ V for the iron–sulfur cluster [8]. Because the two redox potentials for the FAD and the potential for the [4Fe–4S] are so similar, this enzymatic reduced state is a redox equilibrium involving partial reduction of the [4Fe–4S] and of the FAD [3,5,8,9]. A stronger reductant, such as dithionite, is required to reduce the protein to a nominally ''three-electron reduced'' state [3,5,8,9].

ETF–QO presents additional challenges relative to prior studies of methods to determine distances between paramagnetic centers in proteins [10]. Previously, the possibility of dipolar interaction between the anionic semiquinone and $[4Fe–4S]^{+}$ in ETF–QO was suggested [7] and it was noted that a small broadening along one principal axis of the $[4Fe–4S]^{+}$ signal at low temperature could be due to dipolar interaction with paramagnetic semiquinone [7]; however, the changes were too small to be conclusive. The crystal structure of porcine ETF–QO to 2.7-Å resolution shows that the distances of closest approach between the $[4Fe–4S]^{+}$ and the methyl group(8α) of the FAD isoalloxazine ring and between the $[4Fe–4S]^{+}$ and the bound benzoquinone ring of ubiquinone are 11.5 and 18.8 Å, respectively [11]. The point-dipole distance between the unpaired electrons is substantially larger than the distance of closest approach since the semiquinone unpaired spin density is distributed over the FAD molecule [12,13]. The effect of a rapidly relaxing paramagnetic metal center on the electron spin relaxation rate of a more slowly relaxing center can be used to determine interspin distances [14–16]. Enhancement of spin-lattice relaxation has been used to determine distances between sites in photosystems [17], spin-labeled iron porphyrins and heme proteins [18–22], and proteins containing iron–sulfur clusters [23–26]. Relaxation enhancement methods were preferred for these proteins, relative to CW lineshape studies, because the dipolar interaction is small compared to linewidths. Determination of distances using double electron–electron resonance (DEER) [27,28] or double quantum coherence [29] would be very difficult in this system because it is not possible to generate a pulse microwave field (B_1) that is large enough to excite a significant fraction of the signal from the $[4Fe–4S]^{+}$. Application of DEER also is limited by the requirement that the frequencies for the pump and probe pulses are within the bandwidth of the resonator.

This report evaluates spin-lattice relaxation enhancement measured by inversion recovery to determine interspin distances for a system in which the redox potentials do not permit preparation of a sample with both interacting centers exclusively in the paramagnetic state. CW EPR measurements were performed to characterize and quantitate the paramagnetic forms of the redox-active centers. The point-dipole distance between $[4Fe–4S]^{+}$ and the anionic semiquinone was determined for *Rhodobacter*, human, and porcine ETF–QO. A sample of the related protein, electron transfer flavoprotein (ETF), which contains an anionic flavosemiquinone but no iron–sulfur cluster, was studied to determine the relaxation rates for the semiquinone signal in the absence of interaction with the iron–sulfur cluster. For the porcine enzyme the relative locations of the redox cofactors obtained by relaxation enhancement can be compared with the crystal structure data, which provides a validation of the method. Structural information also was obtained for the human and *Rhodobacter* enzymes, for which crystal structures are not available.

2. Experimental

2.1. Purification of ETF–QO proteins

Porcine liver ETF–QO was purified as described by Watmough and co-workers [30]. Human ETF–QO was expressed from a baculovirus vector, expressed in sf9 cells, and purified by the method of Simkovic et al. [3]. The ETF–QO from *R. sphaeroides* was expressed in *Escherichia coli* C43 [31] and purified by the method reported in Usselman et al. [32]. The concentrations of the three proteins were determined spectrophotometrically using $\varepsilon_{430\,nm} = 2.4 \times 10^4\ M^{-1}\,cm^{-1}$ [3,5,9]. The purified proteins do not contain ubiquinone so throughout this manuscript quinone and semiquinone refer to the FAD moiety.

2.2. Reduction of ETF–QO and preparation of EPR samples

The proteins were reduced either enzymatically to generate the two-electron reduced species or with sodium dithionite to generate the three-electron reduced species as previously described [2,3,7]. The proteins, ~30 to 90 μM, were enzymatically reduced in stoppered cuvettes containing 0.1 M Tris–HCl, pH 7.8, 8 mM CHAPS, 40% glycerol, 1 μM human medium-chain acyl-CoA dehydrogenase, 1 μM human electron transfer flavoprotein, and 20 mM β-D-glucose. The reaction mixtures were made anaerobic by 10 cycles of alternate evacuation and purging with nitrogen; residual oxygen was removed by addition of glucose oxidase (1 U/mL) and catalase (24 U/mL) [2]. Octanoyl-CoA was added to give a fourfold molar excess over ETF–QO. Absorption spectra were measured at 10 min intervals until the spectrum was stable for 20–30 min. The three-electron reduced species was generated by reduction with dithionite under similar conditions, but without the other enzymes and acyl-CoA substrate. Dithionite was prepared as a 5 mM solution in anaerobic 0.1 M sodium pyrophosphate, pH 9.0. Glucose oxidase and catalase were added to remove residual oxygen before addition

of dithionite in several aliquots. The absorption spectra of the oxidized, and two- and three-electron reduced species of the *Rhodobacter* protein are shown in Fig. 1. The reduced proteins were transferred anaerobically to 4 mm OD quartz EPR tubes, and the tubes were flame sealed. The solutions were rapidly frozen in liquid nitrogen and stored in liquid nitrogen.

2.3. EPR spectroscopy

CW EPR spectra of the FAD semiquinone signal were recorded at 9.224–9.227 GHz on a Varian E109 spectrometer with a rectangular cavity, a GaAsFET amplifier and a Varian liquid nitrogen-cooled gas flow system. The operating conditions were: 108 K, 4.0 G modulation amplitude at 100 kHz, and a microwave power of 5 μW. Spectra were recorded using 3–12, 200 G scans. The semiquinone concentration was calculated by double integration of the EPR signal and compared to a tempo1 standard (0.80 mM). The operating conditions for the tempol standard were: 108 K, 0.5 G modulation amplitude at 100 kHz, and a microwave power of 5 μW. The tempol standard also was used to determine the concentration (1.4 mM) of a sample of CuEDTA [33] in 1:1 water/glycerol that was used to calculate the concentrations of the paramagnetic $[4Fe–4S]^{+}$. The concentration determined by EPR was in good agreement with the Cu^{2+} concentration calculated by optical spectroscopy of the $CuSO_4$ solution ($\varepsilon_{806\,nm} = 11.74\ M^{-1}\,cm^{-1}$) that was used to prepare the CuEDTA. By calculating the concentrations of both the semiquinone and $[4Fe–4S]^{+}$ signals relative to the same tempol standard, relative concentrations should be more reliable, even if there are uncertainties in the absolute concentrations.

CW EPR spectra of the $[4Fe–4S]^{+}$ were recorded at 9.349–9.5 GHz on either a Bruker E580 spectrometer or a locally-constructed spectrometer [34] with a Bruker split-ring resonator and Oxford CF 935 cryostat. The operating conditions were: 10–45 K, 5.0 G modulation amplitude at 100 kHz, and microwave powers between 0.0016 and 2 mW. The $[4Fe–4S]^{+}$ concentration was calculated by double integration of spectra recorded at 18 and 20 K and compared to signals for the standard sample of CuEDTA at the same temperatures. The operating conditions for the standard were: 5.0 G modulation amplitude at 100 kHz, and microwave powers between 5 and 20 μW. Between 15 and 20 K it is possible to record spectra of the standard in a linear response region and the $[4Fe–4S]^{+}$ signal is sharp enough that integration is more precise than at higher temperature. Spectra were recorded with sweep widths between 850 and 1000 G and averaging of multiple scans. Resonator background spectra of a buffer/glycerol (1:1) solution were recorded under identical conditions and subtracted from spectra of the iron–sulfur cluster. The semiquinone signal overlaps with the $[4Fe–4S]^{+}$ signal (see Fig. 2) so to permit quantitation of the signal from the iron–sulfur cluster, the semiquinone signal was subtracted using a simulated spectrum or by zeroing the semiquinone data pixels in the data file. Double integrals obtained by the two methods agreed within experimental error.

Electron spin echo (ESE) experiments were performed at 10–50 K on a Bruker E580 or a locally-constructed spectrometer [34] with a Bruker split-ring resonator and Oxford CF 935 cryostat. The Q of the over-coupled resonator was ~100. Two pulse spin echo decays were recorded using a $\pi/2$–τ–π–τ–echo sequence with pulse lengths of 40 and 80 ns. The attenuation of the pulses was adjusted to give the maximum echo intensity. Initial values of τ ranged from 152 to 252 ns. Three-pulse inversion recovery experiments were performed using a π–T_{var}–$\pi/2$–τ–π–τ–echo sequence with pulse lengths of 32, 16, and 32 ns. The attenuation of the pulses was adjusted to give the maximum echo. Values of τ and initial T_{var} ranged from 332 to 400 ns and 120 to 200 ns, respectively. Recovery curves were recorded at temperatures between 8 and 18 K along the three principal axes for the $S = \frac{1}{2}$, $[4Fe–4S]^{+}$ signal ($g \sim 1.88$, ~1.94, and ~2.09). The pulse repetition time

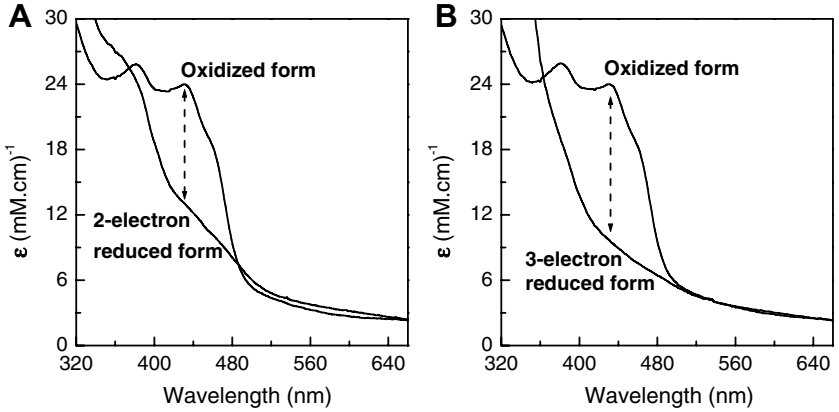

Fig. 1. The absorption spectra of the oxidized, and (A) two- and (B) three-electron reduced species of *Rhodobacter* ETF–QO. The dashed double-ended arrow indicates the wavelength for which the change in molar absorptivity is reported. Samples are in 20 mM Hepes(K^{+}), pH 7.8, containing 30% glycerol. $\Delta\varepsilon_{430\,nm} = 4.9\ mM^{-1}\,cm^{-1}$/electron equivalent.

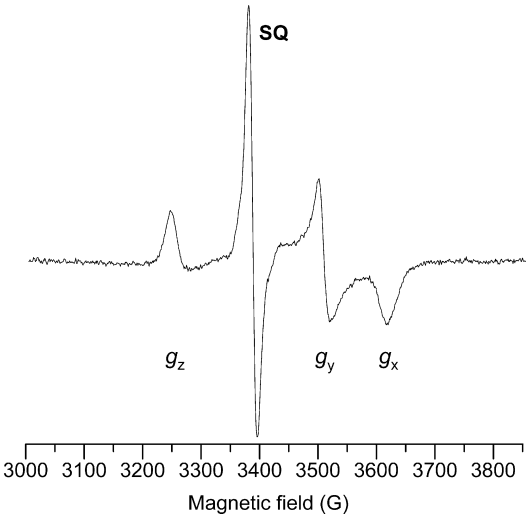

Fig. 2. 9.5 GHz CW spectrum of "three-electron reduced" *Rhodobacter* ETF–QO recorded at 18 K. The sample is in 0.1 M Tris–HCl, pH 7.8, containing 8 mM CHAPS and 40% glycerol. The semiquinone, based on signal intensity at 106 K, is 14% of total protein. At 18 K the microwave power selected to record the $[4Fe–4S]^+$ signal is too high to record an unsaturated semiquinone signal.

was long relative to T_1 and the maximum value of the spacing between the first and second pulses (T_{var}) was selected to permit full recovery of equilibrium magnetization. Background curves recorded for a 1:1 buffer/glycerol sample were subtracted from the two-pulse decay and inversion recovery curves and the amplitude of the background signal was between 1% and 10% at the earliest-time points. In the recovery curves for the $[4Fe–4S]^+$ the contribution of the background signal to the earliest-time points in the recovery curves was as high as 20% for $T_1 < 1$ μs. For the samples of *Rhodobacter* ETF–QO the concentrations of the samples were lower and values of T_1 were shorter such that the resonator background signal makes a more significant contribution to the inversion recovery curves for the $g \sim 2.09$ turning point. Although background signals were subtracted, this data manipulation causes greater uncertainty for the T_1 values measured along this axis. For the semiquinone signal the inversion recovery experiments used 20–80 shots per point, 256 data points, and multiple scans.

2.4. Analysis of CW spectra

Spectra of $[4Fe–4S]^+$ at 10 K were simulated using the program MONMER, which is based on the equations in [35], to determine the *g*-values and the Gaussian first-derivative peak-to-peak linewidths (Table 1). The linewidths of the $[4Fe–4S]^+$ signal are temperature-dependent above about 24 K. The CW spectra from 24 to 45 K were simulated using the locally written program SATMON [36] in which the lineshape is a Gaussian distribution of Lorentzian spin packets characterized by T_2. It was assumed that the distribution widths are independent of temperature. In the temperature range where linewidths are temperature-dependent, it was assumed that $T_1 = T_2$ for $[4Fe–4S]^+$. The uncertainty in T_1 values obtained by this method is ~20% which is caused by imperfect background subtractions and uncertainties in simulations of the broad lines.

2.5. Calculation of relaxation rates

Inversion recovery curves for $[4Fe–4S]^+$ between 8 and 18 K were analyzed first by fitting a single exponential to the data using a nonlinear least-squares algorithm. Provencher's MULTIFIT [37] routine was then used to fit a sum of exponentials to the data, and distinctions between single and multiple exponential fits were based on the statistical tests in the program. The relative weightings for multiple exponential components also were analyzed using Brown's UPEN routines [38,39]. The quality of the fits to the experimental curves was judged from a sum of squares of the residuals. To normalize the residuals, the amplitudes of the recovery curves were scaled to a data range of 0–1.0. Analysis of the data with UPEN found a range of T_1 values based around a most probable value. Values of T_1 calculated using UPEN based on the peak of the distribution, the mid-point of the integral of the peak(s) in the distribution and from the geometric mean of the distribution agreed within 10%. The full widths at half height of the distributions on a logarithmic scale were 0.2–0.6. T_1 values cited in the following discussion are based on UPEN, unless stated otherwise.

The sum of two exponentials (MULTIFIT) or a distribution of exponentials (UPEN) gave better agreement with the inversion recovery curves than was obtained with a single exponential. The values of T_1 found using MULTIFIT fell within the distributions identified by UPEN.

To analyze the shapes of the two-pulse echo decays for $[4Fe–4S]^+$, a stretched exponential (Eq. (1)) was fitted to the data using a Levenberg–Marquardt algorithm:

$$Y(\tau) = Y(0)\exp[-(2\tau/T_m)^x] \quad (1)$$

Table 1
g-Values and linewidths (G) for $[4Fe–4S]^+$ at 15 K

Sample	g_z[a]	Linewidth[b]	g_y[a]	Linewidth[b]	g_x[a]	Linewidth[b]
Rhodobacter	2.089	22	1.934	15	1.875	29
Human	2.082	22	1.938	12	1.886	24
Porcine	2.084	22	1.939	12	1.886	23

[a] The average uncertainty of the *g*-values was ~±0.003.
[b] Peak-to-peak first-derivative linewidths were simulated using MONMER. Average uncertainty of the linewidth was ±1 G. The uncertainties for the g_x and g_y lines in the *Rhodobacter* spectrum is ±2 G.

where $Y(\tau)$ is the intensity of the echo as a function of τ, the time between the two pulses. $Y(0)$, echo intensity extrapolated to time zero, and $Y(\tau)$ are in arbitrary units that depend upon the concentration of the sample, resonator Q, and instrument settings. The parameters x and T_m describe the shape of the echo decay and x depends upon the mechanism of dephasing [40,41]. The decays for the $[4Fe–4S]^+$ showed significant echo envelope modulation. T_m was estimated using an average fit through the decays with $x = 1$.

2.6. Analysis of the temperature dependence of T_1 for $[4Fe–4S]^+$

Parameters in the model shown in Eq. (2) were adjusted to fit the temperature dependence of T_1 for $[4Fe–4S]^+$ that was obtained from a combination of inversion recovery at low temperature and from the temperature-dependent contribution to the CW linewidths at higher temperatures.

$$\frac{1}{T_1} = A_{\mathrm{dir}}T + A_{\mathrm{Ram}}\left(\frac{T}{\theta_{\mathrm{D}}}\right)^9 J_8\left(\frac{\theta_{\mathrm{D}}}{T}\right) + A_{\mathrm{Orb}}\left[\frac{\Delta_{\mathrm{Orb}}^3}{e^{\Delta_{\mathrm{Orb}}/T}-1}\right] \qquad (2)$$

where T is temperature in Kelvin, A_{dir}, A_{Ram}, and A_{Orb} are the coefficients for the contributions from the direct process, the Raman process, and the Orbach process, respectively, θ_{D} is the Debye temperature, J_8 is the transport integral,

$$J_8\left(\frac{\theta_{\mathrm{D}}}{T}\right) = \int_0^{\theta_{\mathrm{D}}/T} x^8 \frac{e^x}{(e^x-1)^2}\,dx,$$

and Δ_{Orb} is the energy separation (in K) between the ground state and the excited state for the Orbach process.

Mathematical expressions for the temperature dependence of spin-lattice relaxation are taken from the following references: direct process [14], Raman process [42,43], and Orbach process [44]. The fit parameters are summarized in Table 2. Based on the original derivations for ionic solids the Orbach energy should be less than the Debye temperature [44]. Bertrand et al. analyzed the temperature dependence of the spin-lattice relaxation rates for [4Fe–4S] proteins and found Orbach energies greater than the Debye temperatures [45]. They showed that the temperature dependence of the relaxation rates predicted for an Orbach process involving local vibrational modes was the same as that for phonons below the Debye limit. They also showed that the Orbach energies determined from the temperature dependence of spin-lattice relaxation were in good agreement with values obtained by magnetic susceptibility [45].

Table 2
Contributions[a] to spin-lattice relaxation of $[4Fe–4S]^+$ in the temperature range 8–45 K

Sample	A_{Ram} (s^{-1})	A_{Orb} ($s^{-1}\,K^{-3}$)	Orbach energy (K)
Rhodobacter	5.8×10^8	2.8×10^4	175
Human	1.1×10^8	1.5×10^4	210
Porcine	0.9×10^8	1.8×10^4	225

[a] Debye temperature = 100 K, coefficients are defined in Eq. (2).

Thus in the analysis of the relaxation rates for the $[4Fe–4S]^+$ cluster the Orbach energy was not constrained to be less than the Debye temperature.

2.7. Simulations to determine interspin distance

2.7.1. Parameters for $[4Fe–4S]^+$ and semiquinone

Analysis of the inversion recovery curves for the semiquinone in the spin-coupled pairs required input of parameters for the $[4Fe–4S]^+$ and semiquinone in the absence of spin–spin interaction. The g-values for the $[4Fe–4S]^+$ and semiquinone were taken from the CW simulations. The spin-lattice relation rates for $[4Fe–4S]^+$ were taken from the fit functions for the temperature dependence of relaxation (Eq. (2)). The distribution width for the $[4Fe–4S]^+$ spin-lattice relaxation rates was selected on the basis of UPEN calculations. At low temperatures electron spin echo decay constants, T_m, for the $[4Fe–4S]^+$ are about 1.5 μs. A variety of processes other than T_2 can contribute to echo dephasing [46]. However, T_2 must be at least as long as T_m so at low temperature T_2 must be greater than about 1.5 μs. At the temperatures where the $[4Fe–4S]^+$ had significant impact on the T_1 for semiquinone, T_1 for the $[4Fe–4S]^+$ is much shorter than 1.5 μs, so it was assumed that T_1 was driving T_2 and that $T_1 = T_2$ for $[4Fe–4S]^+$. Values of T_1 for the semiquinone in the absence of relaxation enhancement were based on measurements for the semiquinone in ETF using the same time window for data acquisition for ETF and ETF–QO at each temperature. In most of the simulations it was assumed that the contribution of electron–electron exchange is negligible compared to dipolar interaction because of the long interspin distances and absence of a direct through-bond interaction pathway in these samples. Addition of a non-zero exchange interaction did not improve the fit between experimental and calculated curves.

2.7.2. Relaxation enhancement

The difference between the inversion recovery curves at 42 K for a two-electron reduced porcine ETF–QO sample and for ETF (Fig. 3) is typical of the substantial enhancement of the semiquinone relaxation rates due to interaction with the rapidly relaxation $[4Fe–4S]^+$. A modified version of the Bloembergen equation [16,21] was used to model the relaxation enhancement and thereby determine the point-dipole distance between the semiquinone and $[4Fe–4S]^+$ cluster. The approach, using the locally written program MENOSR, is similar to that used previously to determine the distance between low-spin or high-spin Fe(III) and nitroxyl for spin-labeled metmyoglobin variants [16]. The relaxation enhancement is calculated for many orientations of the molecule in the magnetic field and contributions are summed to calculate the powder average inversion recovery curve. The calculation assumes a random distribution of molecules in the external magnetic field, but only those for which the semiquinone resonance occurred within a band of 10 G centered at the magnetic

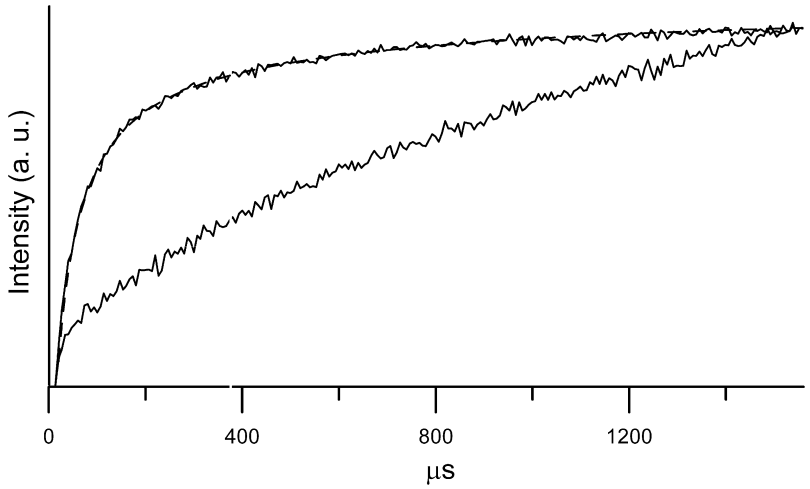

Fig. 3. Inversion recovery curves for two-electron reduced porcine ETF–QO (upper curve) and ETF (lower curve) at 36 K. The dashed line is a simulated curve calculated with MENOSR for an interspin distance of 19 Å. Samples are in 0.1 M Tris–HCl, pH 7.8, containing 8 mM CHAPS and 40% glycerol.

field used for the experiment are included in the calculation. The large magnetic field range for orientation selection was used to account for the extensive unresolved nuclear hyperfine splitting of the semiquinone signal. The inhomogenously broadened first-derivative peak-to-peak line widths for the anionic semiquinone are anisotropic and estimated from the X-band CW spectra at 108 K to be 10, 9, and 21 G at the g_z, g_y, and g_x positions, respectively. The percentage of the paramagnetic $[4Fe–4S]^+$, which is required for the simulations, was obtained by CW quantitation (Table 3). The value of the interspin distance, r, was adjusted to fit the SR curve. Typically, good fits were defined as sum of the squares of the residual <0.03 (see Fig. 3). The effect of the rapidly relaxing iron–sulfur cluster on the semiquinone depends on the orientation of the interspin vector relative to the axes of the cluster. At X-band there is not enough resolution of the semiquinone signal to use orientation selection in the experiments. To test for the impact of the assumed orientation on the estimated interspin distance, simulations were performed for eight orientations, and an average value of r was calculated at each temperature. Distances were calculated only at temperatures where interaction with the $[4Fe–4S]^+$ caused more than a factor of three increase in the semiquinone relaxation rates. The distance values listed in Table 3 are an average for each protein calculated at four temperatures between 31 and 50 K. The uncertainties are the average of standard deviations for the distances calculated at each temperature.

Uncertainty in the $[4Fe–4S]^+$ relaxation rates could be a systematic source of error in the distances. The relaxation rates were taken from the fit functions which included interpolation between 18 and 40 K and extrapolation above about 40 K. The estimated error in r for a factor of 2 increase/decrease in $[4Fe–4S]^+$ T_1 is approximately ± 1.2 Å. Variation of the $[4Fe–4S]^+$ T_1 distribution width from 0 to 0.60 on a logarithmic scale made a -0.8 Å distance change. Uncertainty in experimental temperature (± 1 K) also is a source of systematic error. A further source of systematic error may arise from the impact of spectral diffusion on the inversion recovery curves (see Section 3) of the semiquinone signal. The magnitude of the contribution from spectral diffusion is unknown. However, relaxation enhancement dominates relaxation rates for the semiquinone in ETF–QO between 30 and 50 K and calculated curves were not strongly impacted by increasing the T_1 estimated for the semiquinone by a factor of 2.

When interspin distance measurements were made for spin-labeled iron porphyrins [19,20,22,36] all of the heme was paramagnetic, but in the reduced ETF–QO samples part of the [4Fe–4S] is diamagnetic. Because the relaxation enhancement is so large, the contributions to the inversion recovery curves from semiquinone with a neighboring diamagnetic $[4Fe–4S]^{2+}$ cluster contributed primarily at the long-time extreme of the experimental data and made little difference at short times where relaxation enhancement

Table 3
Quantitation and spin–spin distances

Sample	Redox state	% SQ[a]	% $[4Fe–4S]^+$[b]	r[c] (Å)
Rhodobacter	Two-electron[d]	44	83	18.7 ± 0.6
Rhodobacter	Three-electron[e]	14	90	19.6 ± 0.6
Human	Two-electron[d]	24	60	17.6 ± 0.7
Porcine	Two-electron[d]	29	87	17.9 ± 1.0
Porcine	Three-electron[e]	11	88	19.0 ± 0.6

[a] Determined using double integration of the semiquinone CW spectra relative to tempol standard, for multiple sample preparations. The percentages are relative to the total protein concentration. Values are accurate to ±5%.

[b] Determined using double integration of the $[4Fe–4S]^+$ cluster CW spectra relative to CuEDTA standard. The percentages are an average from duplicate measurements at 18 and 20 K and are relative to the total protein concentration. Values accurate to ±10%.

[c] Calculated using MENOSR. Uncertainties are the standard deviations of distances calculated at four temperatures between 31 and 50 K.

[d] Enzymatically reduced.

[e] Dithionite reduced.

dominates. The agreement between the experimental and calculated inversion recovery curves was quite sensitive to the value of r, particularly for the early time data. For example, for one two-electron reduced data set a ±1.0 Å change from the best-fit distance caused the sum of the squares of the residuals (SSQ) to increase from 0.016 to 0.044. The values of r that gave the best agreement were not very sensitive to the fraction of $[4Fe–4S]^{+}$. For the two-electron reduced samples a 25–30% variation in the concentration of $[4Fe–4S]^{+}$ produced good fits to the curves (SSQ < 0.03) with only a small change of distance, ~0.3 Å. In the three-electron reduced samples the fraction of $[4Fe–4S]^{+}$ is larger than for the two-electron reduced samples, which decreases the contribution from semiquinone that does not have enhanced relaxation rates. For the three-electron reduced samples the agreement between experimental data and simulation is more sensitive to the orientation of the interspin vector relative to the axes of the iron–sulfur cluster, which is attributed to the smaller contribution from semiquinone with a neighboring diamagnetic iron–sulfur cluster. However, the differences in quality of fit were not large enough to define the orientation of the interspin vector relative to the axes of the $[4Fe–4S]^{+}$. The lower concentrations of semiquinone in the three-electron reduced samples made it more difficult to achieve acceptable signal-to-noise in the inversion recovery curves.

3. Results and discussion

3.1. g-Values and linewidths

The g-values and linewidths at 15 K for the ETF–QO $[4Fe–4S]^{+}$ signal from the three species are displayed in Table 1. The g-values are in good agreement with literature values for porcine ETF–QO [1,3,7] and for other $[4Fe–4S]^{+}$ [47,48]. Low-temperature linewidths were broader at the g_x and g_y turning points in the EPR spectra of the *Rhodobacter* samples than for the human and porcine samples (Table 1 and Fig. 4), which may be the result of greater unresolved hyperfine couplings and/or distributions in g- and A-values.

3.2. Electron spin-lattice relaxation rates, $1/T_1$, for $[4Fe–4S]^{+}$

The temperature dependence of the relaxation rates of $[4Fe–4S]^{+}$ are displayed in Fig. 5 for two-electron reduced samples. At all temperatures studied, the relaxation rates for $[4Fe–4S]^{+}$ in the *Rhodobacter* protein are faster than for the human and porcine proteins. Within experimental uncertainty values of T_1 measured at the g_y turning point were the same for two-electron and three-electron reduced samples. This position in the spectrum was selected for the comparison because the signal-to-noise is the best. The spin-lattice relaxation rates were weakly anisotropic and $1/T_1$ between 8 and 18 K for the mammalian proteins

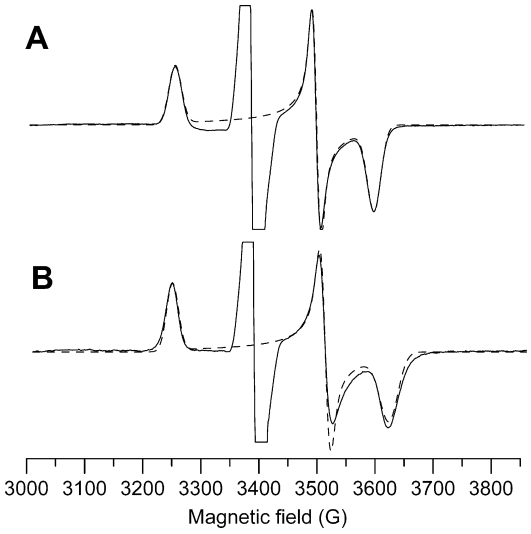

Fig. 4. 9.49 GHz CW spectra of two-electron reduced porcine (A) and *Rhodobacter* (B) ETF–QO recorded at 15 K. The samples are in 0.1 M Tris–HCl, pH 7.8, containing 8 mM CHAPS and 40% glycerol. Dashed lines are simulations calculated using the program MONMER.

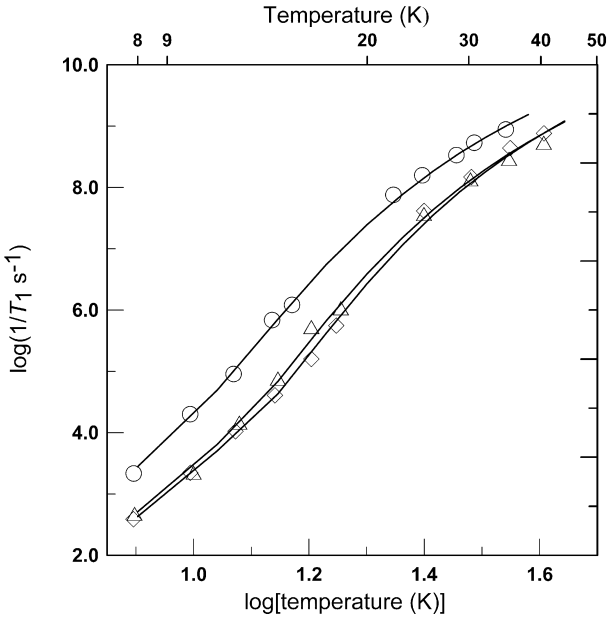

Fig. 5. Temperature dependence of spin-lattice relaxation rates for two-electron reduced $[4Fe–4S]^{+}$ in *Rhodobacter* (○), porcine (◇), and human (△) ETF–QO. Values were measured by inversion recovery (8–16 K) or calculated from the temperature contribution to the lineshape (22 to ~40 K). The values of T_1 are averages along the g_x, g_y, and g_z turning points. The solid lines through the data are the fit functions calculated using the model in Eq. (2) and the parameters in Table 2. Samples are in 0.1 M Tris–HCl, pH 7.8, containing 8 mM CHAPS and 40% glycerol.

increases in the order $1/T_1(g_x) < 1/T_1(g_z) < 1/T_1(g_y)$. The anisotropy was up to 60% at the lowest temperatures measured, which is small relative to the distribution widths. Distributions in relaxation rates have also been observed for Cu(II) [49] and V(IV) [50] complexes and may be due to distributions in structures and electronic energies analo-

gous to the well-documented phenomenon of *g*- and *A*-strain [51]. Anisotropy of $1/T_1$ between 30 and 50 K also has been found in 4Fe–4S ferredoxins [52].

Parameters in Eq. (2) were adjusted to fit the temperature dependence of $1/T_1$ and the best-fit parameters are summarized in Table 2. Similar values were obtained by analysis of relaxation rates along g_x, g_y, and g_z individually or orientation-averaged. The Raman process dominated spin-lattice relaxation between 8 and 16 K. The Debye temperatures obtained from fits to the temperature dependence of $1/T_1$ are similar for the three proteins. There is substantial uncertainty in the value of the Debye temperature because of the overlapping contributions from the direct process. Values of the coefficient for the Raman process, A_{Ram}, and the Debye temperature (θ_{D}, Eq. (2)) are correlated. To facilitate comparisons, the Debye temperature was fixed at 100 K and the coefficient A_{Ram} was adjusted (Table 2). The faster relaxation for the $[4Fe–4S]^{+}$ in the *Rhodobacter* protein is reflected in the larger value of A_{Ram}. Literature values of Debye temperatures for protein samples include 78–82 K for low-spin heme iron in the methylimidazole and cyanide adducts of horse heart myoglobin in water/glycerol [53], 60 K for 2-iron–2-sulfur ferredoxin of the blue green alga *Spirulina maxima* in Tris buffer [54], and 60 K for the [4Fe–4S] ferredoxin from *Bacillus stearothermophilus* in Tris buffer [45]. The Orbach energies for human and porcine ETF–QO are within experimental error of each other (210–225 K). The Orbach energy is lower for the *Rhodobacter* ETF–QO (175 K) than for the human and porcine proteins, which indicates a lower-lying excited state for the *Rhodobacter* protein than for the human and porcine proteins. The Orbach energies are comparable to values obtained for reduced [4Fe–4S] ferredoxins [45,52] (144–432 K, 100–300 cm^{-1}).

3.3. Formation of paramagnetic $[4Fe–4S]^{+}$

The reduction potentials for the quinone–semiquinone–hydroquinone and $[4Fe–4S]^{2+,1+}$ couples are sufficiently close together that the reduction steps overlap [5,8]. In the ''two-electron'' reduced protein only part of the quinone is in the semiquinone form and there is a mixture of the +1 and +2 oxidation states of the [4Fe–4S] cluster. In the ''three-electron'' reduced protein most of the [4Fe–4S] cluster is paramagnetic, and most of the quinone has been reduced to diamagnetic hydroquinone. The relaxation enhancement for the semiquinone occurs only for the subset of semiquinones for which the neighboring iron–sulfur cluster is paramagnetic, which means that the fraction of [4Fe–4S] in the paramagnetic form +1 oxidation state is a parameter in the data analysis.

For the two-electron reduced samples the percentage of $[4Fe–4S]^{+}$ for the three proteins (Table 3) determined by quantitation of the CW EPR signal was 60–87%, which is within experimental uncertainty of the 72% reported for porcine ETF–QO [7]. In the three-electron reduced samples the percentage of $[4Fe–4S]^{+}$ increased to 88–90% which also agrees well with the 84% reported previously for the porcine protein [7]. Thus, less than 100% of the iron–sulfur cluster is in the paramagnetic $[4Fe–4S]^{+}$ form even in the nominally three-electron reduced samples, which may reflect the difficulty in forcing redox equilibria to completion. The similarity between the EPR signal quantitations for the three proteins is consistent with similar reduction potentials for the iron–sulfur clusters.

The spin-coupling between the 4 iron atoms of the [4Fe–4S] cluster produces a series of excited states [48]. For $[4Fe–4S]^{2+}$ although the ground state is diamagnetic, there are paramagnetic excited states. Similarly for $[4Fe–4S]^{+}$ there are excited states with $S > 1/2$. Fluid solution NMR studies have shown that population of these excited states is significant at temperatures near 298 K [48]. If population of these excited states were significant at 30–50 K where the relaxation enhancement measurements of interspin distances were performed, then omission of these states from the model for relaxation enhancement would cause the apparent distance to increase with increasing temperature. Since this trend was not observed, it was assumed that the contributions of excited states to relaxation enhancement could be neglected.

The percentage of semiquinone for two-electron reduced porcine (29%), human (24%), and *Rhodobacter* (44%) ETF–QO (Table 2) found in this study are lower than previously reported (60%) for a two-electron reduced porcine sample [8]. Calculations of the equilibrium concentrations of the redox active species, based on the literature values of the reduction potentials for porcine ETF–QO [8], predict a maximum of 50% semiquinone when 1.7 electrons have been added. For the two-electron reduced samples the observed % semiquinone should be less than the maximum value due to addition of more electrons and increased reduction to hydroquinone. Thus the observations in this study of percentages less than 50% are consistent with the reported redox potentials. The somewhat higher percentage of semiquinone for the two-electron reduced *Rhodobacter* sample than for porcine or human samples suggests small differences in redox potentials. In the three-electron reduced samples the % semiquinone decreases to 6–11% for the *Rhodobacter* and porcine protein, respectively. Based on the literature values of the reduction potentials, the calculated equilibrium concentrations of $[4Fe–4S]^{+}$ are ~85% and ~99% when two- and three-electrons have been added, respectively. The CW quantitation results (Table 2) agree within experimental error with these values.

3.4. Use of ETF as model for non-interacting FAD semiquinone

ETF was employed as the model for anionic flavin semiquinone in the absence of interaction with a paramagnetic iron sulfur cluster. Both ETF–QO and ETF contain FAD in an extended conformation [11,55] and both stabilize an

anionic semiquinone with very similar EPR line widths, 14.5 G for ETF [56] and 14.6 G for porcine ETF–QO [7].

3.5. Saturation recovery vs. inversion recovery for T_1 measurements

Inversion recovery was used to measure relaxation rates of these protein samples because the signal-to-noise for inversion recovery curves is significantly better than for saturation recovery (SR) for samples with low concentrations. In the inversion recovery experiments essentially all of the spins within the bandwidth of the over-coupled resonator are flipped by the inverting pulse and contribute to the recovery curve. In SR only a weakly perturbing B_1 can be used to monitor the smaller number of spins that are within the bandwidth of the critically-coupled high-Q resonator. However, the inversion recovery curves may be susceptible to the effects of spectral diffusion because the inverting pulse is so short, whereas in a SR experiment the long saturating pulse decreases the contributions from spectral diffusion. The term spectral diffusion [57,58] refers to all processes that move spin magnetization between positions in the EPR spectrum. If spectral diffusion moves an excited spin outside the detection window for the experiment, this process is an apparent relaxation process and will result in a shorter measured value of T_1 [58]. Spectral diffusion is more likely to contribute to the inversion recovery curves for the slowly relaxing semiquinone signal than the much faster relaxing $[4Fe–4S]^+$. Because the effect of the $[4Fe–4S]^+$ is so large relative to the contributions from spectral diffusion between 30 and 50 K, the better signal-to-noise and shorter dead-time of the inversion recovery experiment makes inversion recovery a more reliable method to determine relaxation enhancement for these samples. Spectral diffusion could be a greater concern for samples with longer r and/or smaller relaxation enhancement.

The inversion recovery curves for the semiquinone in ETF–QO are superpositions of contributions from radicals with a neighboring diamagnetic $[4Fe–4S]^{2+}$ cluster and radicals with a neighboring paramagnetic $[4Fe–4S]^+$ cluster. The inversion recovery data focused on the contributions from the more rapidly relaxing semiquinone that was interacting with the $[4Fe–4S]^+$ cluster by making the length of the data acquisition time window shorter than would be used to record the full return to equilibrium of the signal for the semiquinone in both environments. Spectral diffusion probably makes a significant contribution to the inversion recovery curves for the semiquinone in ETF. However, by keeping the data acquisition window for the recovery curves for semiquinone in ETF and in ETF–QO the same at each temperature studied, the contributions from spectral diffusion are assumed to remain constant and to not interfere with the distance measurements.

If the pulse repetition time (SRT) is short relative to the T_1 for some components of a distribution, those components are under-represented in the experimental data. Since T_1 is much longer for semiquinone with a neighboring diamagnetic iron–sulfur cluster, the selection of the SRT value impacts the amplitude of the contribution from these sites. To determine the sensitivity of the distance measurements to the value of SRT, inversion recovery curves were recorded with two different selection criteria for SRT—either SRT equal to the window length for data acquisition or 5–10 times the window length. In both cases the SRT is shorter than would be selected to acquire inversion recovery curves for semiquinone in the absence of interaction with the paramagnetic $[4Fe–4S]^+$ cluster. The values of r obtained by analysis with MENOSR were independent of SRT.

3.6. Iron–semiquinone interspin distances

The $[4Fe–4S]^+$–semiquinone interspin distances obtained for the three protein samples by analysis of the semiquinone inversion recovery curves using MENOSR are between 17.6 ± 1 and 19.6 ± 1 Å (Table 3). The similarity in distances is consistent with expectations that the structures of these proteins are very similar. The calculated distances are the same, within estimated uncertainties for the two- and three-electron reduced samples which indicates that the differences in the fraction of interacting $[4Fe–4S]^+$ are satisfactorily taken into account in the data analysis.

The point-dipole values of r (Table 3) are "effective" distances between the average positions of the delocalized spin densities on the semiquinone and on the iron–sulfur cluster. To relate these distances to the X-ray crystal structure [11] it is necessary to consider the spin density distributions. ENDOR (electron nuclear double resonance) measurements of nuclear hyperfine couplings for anionic semiquinones in protein and model compounds [12] permit calculation of the unpaired electron spin density distributions [13]. The largest spin densities are on nitrogen atoms of the central pyrazine ring [N(10) and N(5) positions] and at the C(8) position on the benzenoid ring. The spin on the anionic semiquinone can be approximated as a point-dipole located at the barycenter of its spin density, which is about 4.5 Å from the methyl group(8α). In the $[4Fe–4S]^+$ the unpaired spin is not equally distributed over the four iron atoms. The delocalization of the magnetic moment is determined by strong intracluster exchange coupling. Bertrand et al. developed a local spin model suited for valence-localized clusters [59] and a local model for a cluster that contains partially or completely delocalized mixed-valence pairs [60]. The X-band EPR spectrum of trimethylamine dehydrogenase was simulated using a local spin Hamiltonian to describe the dipolar interactions between the semiquinone radical and the four iron sites of the $[4Fe–4S]^+$ cluster where the nearest atoms of the two centers are separated by 4 Å [23]. In this case the angles between the external magnetic field and the vectors from the semiquinone to individual iron atoms are very different, which makes the dipolar couplings to individual iron atoms very different. The interspin distance between $[4Fe–4S]^+$ and semiquinone in ETF–QO of ~19 Å is sufficiently long that the individual semiquinone–iron vectors make similar angles with respect to the external field and dipolar cou-

plings to the four iron atoms are more similar. The uncertainty arising from the delocalization of the magnetic moment in $[4Fe–4S]^+$ is smaller at the longer distance and the average position for the spin density on the cluster can be taken as the center of the tetrahedron that the iron atoms form. Fee et al. [61] calculated the cluster radius to be between 1.66 and 1.69 Å based on analysis of circumspheres for 12 high-resolution structures of protein-bound and small molecule $[4Fe–4S](SR)_4$ clusters.

The X-ray structure for porcine ETF–QO [11] shows that the orientation of the semiquinone with respect to the axes of the cluster is end-on and the distance of closest approach is 11.5 Å between the iron–sulfur cluster and the methyl group(8α) of the flavosemiquinone. Based on the considerations in the previous paragraph, two corrections need to be applied to the point-dipole distance. The methyl group(8α) is about 4.5 Å from the center of spin density for the semiquinone and an individual Fe atom is about 1.7 Å from the center of the iron tetrahedron. Subtraction of 6.2 Å from the average point-dipole distance of 18.6 ± 1 Å gives an estimated distance of closest approach of 12.4 ± 1 Å, which is in reasonable agreement with the value of 11.5 Å in the crystal structure.

4. Conclusion

EPR *g*-values, linewidths, electron spin-lattice relaxation rates, and Orbach energies for the paramagnetic $[4Fe–4S]^+$ in porcine, human and *R. sphaeroides* ETF–QO are similar, which indicates substantial similarity in electronic structure and is consistent with the high sequence homology. Although it is probable that spectral diffusion contributes to the effective relaxation rates that are measured by inversion recovery for the semiquinone, by keeping the time window for acquisition of the inversion recovery data the same for the reference ETF sample and for the ETF–QO sample, it was possible to characterize the relaxation enhancement. The enhancement of the semiquinone relaxation by the rapidly relaxing $[4Fe–4S]^+$ at a point-dipole distance of about 18.6 Å is large enough that it also is relatively straightforward to distinguish the contribution to the inversion recovery curves from semiquinone with a neighboring diamagnetic $[4Fe–4S]^{2+}$ vs. paramagnetic $[4Fe–4S]^+$. The point-dipole distances between the semiquinone and $[4Fe–4S]^+$ obtained by analysis of the relaxation enhancement are 18.6 ± 1 Å for the three proteins, which is within experimental error of the value calculated based on the crystal structure of porcine ETF–QO when spin delocalization is taken into account.

Acknowledgments

Support of this work by NIH/NIBIB EB002807 (GRE and SSE) and HD08315 (FF), and by the BBRSC Underwood Fund (NW) is gratefully acknowledged.

References

[1] F.J. Ruzicka, H. Beinert, A new iron–sulfur protein of the respiratory chain: a component of the fatty acid oxidation pathway, J. Biol. Chem. 252 (1977) 8440–8445.
[2] J.D. Beckmann, F.E. Frerman, Reaction of electron transfer flavoprotein with electron transfer flavoprotein–ubiquinone oxidoreductase, Biochemistry 24 (1985) 3922–3925.
[3] M. Simkovic, G.D. Degala, S.S. Eaton, F.E. Frerman, Expression of human electron transfer flavoprotein–ubiquinone oxidoreductase from a baculovirus vector: kinetic and spectral characterization of the human protein, Biochem. J. 364 (2002) 659–667.
[4] S.I. Goodman, K. Axtel, L.A. Bindoff, S.E. Beard, R.E. Gill, F.E. Frerman, Molecular cloning and expression of a cDNA encoding human electron transfer flavoprotein–ubiquinone oxidoreductase, Eur. J. Biochem. 219 (1994) 277–286.
[5] N.J. Watmough, F.E. Frerman, J.N. Butt, unpublished results (2007).
[6] C. Chothia, A.M. Lesk, The relation between the divergence of sequence and structure in proteins, EMBO J. 5 (1986) 823–826.
[7] M.K. Johnson, J.E. Morningstar, M. Oliver, F.E. Frerman, Electron paramagnetic resonance and magnetic circular dichroism studies of electron-transfer flavoprotein–ubiquinone oxidoreductase from pig liver, FEBS Lett. 226 (1987) 129–133.
[8] K.E. Paulsen, A.M. Orville, F.E. Frerman, J.D. Lipscomb, M.T. Stankovich, Redox properties of electron-transfer flavoprotein–ubiquinone oxidoreductase as determined by EPR-spectroelectrochemistry, Biochemistry 31 (1992) 11755–11761.
[9] J.D. Beckmann, F.E. Frerman, Electron transfer flavoprotein–ubiquinone oxidoreductase from pig liver: purification and molecular, redox and catalytic properties, Biochemistry 24 (1985) 3913–3921.
[10] L.J. Berliner, G.R. Eaton, S.S. Eaton, Distance Measurements in Biological Systems by EPR, Kluwer, New York, 2000.
[11] J. Zhang, F.E. Frerman, J.-J. Kim, Structure of electron transfer flavoprotein–ubiquinone oxidoreductase and electron transfer to the mitochondrial ubiquinone pool, Proc. Natl. Acad. Sci. USA 103 (2006) 16212–16217.
[12] D.E. Edmondson, Electron-spin-resonance studies on flavoenzymes, Biochem. Soc. Trans. 13 (1985) 593–600.
[13] J.I. Garcia, M. Medina, J. Sancho, P.J. Alonso, C. Gomez-Morena, J.A. Mayoral, J.I. Martinez, Theoretical analysis of the electron spin density distribution of the flavin semiquinone isoalloxazine ring within model protein environments, J. Phys. Chem. A 106 (2002) 4729–4735.
[14] C.P. Poole, H. Farach, Relaxation in Magnetic Resonance, Academic Press, New York, 1971.
[15] A.V. Kulikov, G.I. Likhtenshtein, The use of spin relaxation phenomena in the investigation of the structure of model and biological systems by the method of spin labels, Adv. Mol. Relax. Interact. Proc. 10 (1977) 47–69.
[16] S.S. Eaton, G.R. Eaton, Determination of distances based on T_1 and T_m effects, Biol. Magn. Reson. 19 (2000) 347–381.
[17] K.V. Lakshmi, G.W. Brudvig, Pulsed electron paramagnetic resonance methods for macromolecular structure determination, Curr. Opin. Struct. Biol. 11 (2001) 523–531.
[18] M.H. Rakowsky, K.M. More, A.V. Kulikov, G.R. Eaton, S.S. Eaton, Time-domain electron paramagnetic resonance as a probe of electron–electron spin–spin interaction in spin-labeled low-spin iron porphyrins, J. Am. Chem. Soc. 117 (1995) 2049–2057.
[19] Y. Zhou, B.E. Bowler, G.R. Eaton, S.S. Eaton, Electron spin-lattice relaxation rates for high-spin Fe(III) complexes in glassy solvents at temperatures between 6 and 298 K, J. Magn. Reson. 144 (2000) 115–122.
[20] Y. Zhou, B.E. Bowler, K. Lynch, S.S. Eaton, G.R. Eaton, Interspin distances in spin-labeled metmyoglobin variants determined by saturation recovery EPR, Biophys. J. 79 (2000) 1039–1052.

[21] V. Budker, J.-L. Du, M. Seiter, G.R. Eaton, S.S. Eaton, Electron–electron spin–spin interaction in spin-labeled low-spin methemoglobin, Biophys. J. 68 (1995) 2531–2542.
[22] M. Seiter, V. Budker, J.-L. Du, G.R. Eaton, S.S. Eaton, Interspin distances determined by time domain EPR of spin-labeled high-spin methemoglobin, Inorg. Chim. Acta 273 (1998) 354–366.
[23] A. Fournel, S. Gambarelli, B. Guigliarelli, C. More, M. Asso, G. Chouteau, R. Hille, P. Bertrand, Magnetic interactions between a $[4Fe–4S]^+$ cluster and a flavin mononucleotide radical in the enzyme trimethylamine dehydrogenase: a high-field electron paramagnetic resonance study, J. Chem. Phys. 109 (1998) 10905–10913.
[24] B. Guigliarelli, C. More, A. Fournel, M. Asso, E.C. Hatchikian, R. Williams, R. Cammack, P. Bertrand, Structural organization of the Ni and (4Fe–4S) centers in the active form of *desulfovibrio gigas* hydrogenase. Analysis of the magnetic interactions by electron paramagnetic resonance spectroscopy, Biochemistry 34 (1995) 4781–4790.
[25] R.C. Stevenson, W.R. Dunham, R.H. Sands, T.P. Singer, H. Beinert, Studies on the spin–spin interaction between flavin and iron–sulfur cluster in an iron–sulfur flavoprotein, Biochim. Biophys. Acta 869 (1986) 81–88.
[26] A.D. Vinogradov, V.D. Sled, D.S. Burbaev, V.G. Grivennikova, I.A. Moroz, T. Ohnishi, Energy-dependent complex I-associated ubisemiquinones in submitochondrial particles, FEBS Lett. 370 (1995) 83–87.
[27] G. Jeschke, C. Wegener, M. Nietschke, H. Jung, H.-J. Steinhoff, Interresidual distances determined by four-pulse double electron–electron resonance in an integral membrane protein: the Na^+/proline transporter PutP of *Escherichia coli*, Biophys. J. 86 (2004) 2551–2557.
[28] G. Jeschke, Electron paramagnetic resonance: recent development and trends, Curr. Opin. Solid State Mater. Sci. 7 (2003) 181–188.
[29] P.P. Borbat, J.H. Freed, Double-quantum ESR and distance measurements, Biol. Magn. Reson. 19 (2000) 383–459.
[30] N.J. Watmough, J.P. Loehr, S.K. Drake, F.E. Frerman, Tryptophan fluorescence in electron transfer flavoprotein–ubiquinone oxidoreductase: quenching by a brominated pseudosubstrate, Biochemistry 30 (1991) 1317–1323.
[31] B. Miroux, J.E. Walker, Overproduction of proteins in *Escherichia coli*: mutant hosts that allow synthesis of some membrane proteins and globular proteins at high levels, J. Mol. Biol. 260 (1996) 289–298.
[32] R.J. Usselman, A.J. Fielding, F.E. Frerman, G.R. Eaton, S.S. Eaton, Impact of mutations on the midpoint potential of the $[4Fe–4S]^+$ cluster and on the catalytic activity in electron transfer flavoprotein–ubiquinone oxidoreductase (ETF–QO), Biochemistry, accepted for publication.
[33] K.M. More, G.R. Eaton, S.S. Eaton, Metal-nitroxyl interactions. 47. EPR spectra of two-spin-labeled derivatives of EDTA coordinated to paramagnetic metal ions, Inorg. Chem. 25 (1986) 2638–2646.
[34] R.W. Quine, G.R. Eaton, S.S. Eaton, Pulsed EPR spectrometer, Rev. Sci. Instrum. 58 (1987) 1709–1723.
[35] A.D. Toy, S.H.H. Chaston, J.R. Pilbrow, T.D. Smith, Electron spin resonance study of the copper(II) chelates of certain monothio-β-diketones and diethyldithiocarbamate, Inorg. Chem. 10 (1971) 2219–2225.
[36] M.H. Rakowsky, A. Zecevic, G.R. Eaton, S.S. Eaton, Determination of high-spin iron(III)-nitroxyl distances in spin-labeled porphyrins by time-domain EPR, J. Magn. Reson. 131 (1998) 97–110.
[37] S.W. Provencher, An eigenfunction expansion method for the analysis of exponential decay curves, J. Chem. Phys. 64 (1976) 2772–2777.
[38] G.C. Borgia, R.J.S. Brown, P. Fantazzini, Uniform-penalty inversion of multiexponential decay data, J. Magn. Reson. 132 (1998) 65–77.
[39] G.C. Borgia, R.J.S. Brown, P. Fantazzini, Uniform-penalty inversion of multiexponential decay data II. Data spacing, T_2 data, systematic errors, and diagnostics, J. Magn. Reson. 147 (2000) 273–285.
[40] I.M. Brown, Electron spin echo studies of relaxation processes in molecular solids, in: L. Kevan, R.N. Schwartz (Eds.), Time Domain Electron Spin Resonance, John Wiley, New York, 1979, pp. 195–229.
[41] K.M. Salikhov, Y.D. Tsvetkov, Electron spin-echo studies of interactions in solids, in: L. Kevan, R.N. Schwartz (Eds.), Time Domain Electron Spin Resonance, Wiley, New York, 1979, pp. 232–277.
[42] A. Abragam, The Principles of Nuclear Magnetism, Oxford University Press, Oxford, 1961.
[43] J. Murphy, Spin-lattice relaxation due to local vibrations with temperature-independent amplitudes, Phys. Rev. 145 (1966) 241–247.
[44] R. Orbach, On the theory of spin-lattice relaxation in paramagnetic salts, Proc. Phys. Soc. (Lond.) 77 (1961) 821–826.
[45] P. Bertrand, J.P. Gayda, K.K. Rao, Electron spin-lattice relaxation of the 4Fe–4S ferredoxin from *Bacillus stearothermophilus*. Comparison with other iron proteins, J. Chem. Phys. 76 (1982) 4715–4719.
[46] A. Zecevic, G.R. Eaton, S.S. Eaton, M. Lindgren, Dephasing of electron spin echoes for nitroxyl radicals in glassy solvents by non-methyl and methyl protons, Mol. Phys. 95 (1998) 1255–1263.
[47] H. Beinert, R.H. Sands, Biological applications of EPR involving iron, in: G.R. Eaton et al. (Eds.), Foundations of Modern EPR, World Scientific, Singapore, 1996, pp. 379–409.
[48] I. Bertini, S. Ciurli, C. Luchinat, The electronic structure of FeS centers in proteins and models. A contribution to the understanding of their electron transfer properties, Struct. Bond. 83 (1995) 1–53.
[49] A.J. Fielding, S. Fox, G.L. Millhauser, M. Chattopadhyay, P.M.H. Kroneck, G. Fritz, G.R. Eaton, S.S. Eaton, Electron spin relaxation of copper(II) complexes in glassy solution between 10 and 120 K, J. Magn. Reson. 179 (2006) 92–104.
[50] A.J. Fielding, D.B. Back, M. Engler, B. Baruah, D.C. Crans, G.R. Eaton, S.S. Eaton, Electron spin lattice relaxation of V(IV) complexes in glassy solutions between 15 and 70 K, ACS symposium series, 974 (2007) 364–375.
[51] W. Froncisz, J.S. Hyde, Broadening by strains of lines in the g-parallel region of copper (2+) ion EPR spectra, J. Chem. Phys. 73 (1980) 3123–3131.
[52] J.P. Gayda, P. Bertrand, C. More, J. LeGall, R.C. Cammack, Energy of the low-lying excited levels for some reduced [4Fe–4S] ferrodoxins, from the relaxation broadening of the EPR signals, Biochem. Biophys. Res. Commun. 99 (1981) 1265–1270.
[53] Y. Zhou, B.E. Bowler, G.R. Eaton, S.S. Eaton, Electron spin lattice relaxation rates for $S = 1/2$ molecular species in glassy matrices or magnetically dilute solids at temperatures between 10 and 300 K, J. Magn. Reson. 139 (1999) 165–174.
[54] J.P. Gayda, P. Bertrand, A. Deville, C. More, G. Roger, J.F. Gibson, R. Cammack, Temperature dependence of the electronic spin-lattice relaxation time in a 2-iron–2-sulfur protein, Biochim. Biophys. Acta 581 (1979) 15–26.
[55] D.L. Roberts, F.E. Frerman, J.-J.P. Kim, Three dimensional structure of human electron transfer flavoprotein to 2.1 Å resolution, Proc. Natl. Acad. Sci. USA 93 (1996) 143555–143560.
[56] M.C. McKean, R.C. Sealy, F.E. Frerman, ESR and ENDOR studies on sarcosine dehydrogenase, acyl-CoA dehydrogenase and electron transfer flavoproteins, in: V. Massey, C.H. Williams Jr. (Eds.), Flavins and Flavoproteins, Elsevier, New York, 1982, pp. 614–617.
[57] M.K. Bowman, L. Kevan, Time domain electron spin resonance, in: L. Kevan, R.N. Schwartz (Eds.), John Wiley, New York, 1979.
[58] S.S. Eaton, G.R. Eaton, Relaxation times of organic radicals and transition metal ions, Biol. Magn. Reson. 19 (2000) 29–154.
[59] P. Bertrand, C. More, B. Guigliarelli, A. Fournel, B. Bennett, B. Howes, Biological polynuclear clusters coupled by magnetic interactions: from the point dipole approximation to a local spin model, J. Am. Chem. Soc. 116 (1994) 3078–3086.
[60] P. Bertrand, P. Camensuli, C. More, B. Guigliarelli, A local spin model to describe the magnetic interactions in biological molecules containing $[4Fe–4S]^+$ clusters. Applications to Ni–Fe hydrogenases, J. Am. Chem. Soc. 118 (1996) 1426–1434.
[61] J.A. Fee, J.M. Castagnetto, D.A. Case, L. Noodleman, C.D. Stout, R.A. Torres, The circumsphere as a tool to assess distortion in [4Fe–4S] atom clusters, J. Biol. Inorg. Chem. 8 (2003) 519–526.